

Define:

$$E(z) = [\Omega_M(1+z)^3 + \Omega_k(1+z)^2 + \Omega_\Lambda]^{1/2}$$

Lookback Time:

$$t(z) = \int_0^a \frac{da}{\dot{a}} = \frac{1}{H_o} \int_z^\infty \frac{dz}{(1+z) E(z)}$$

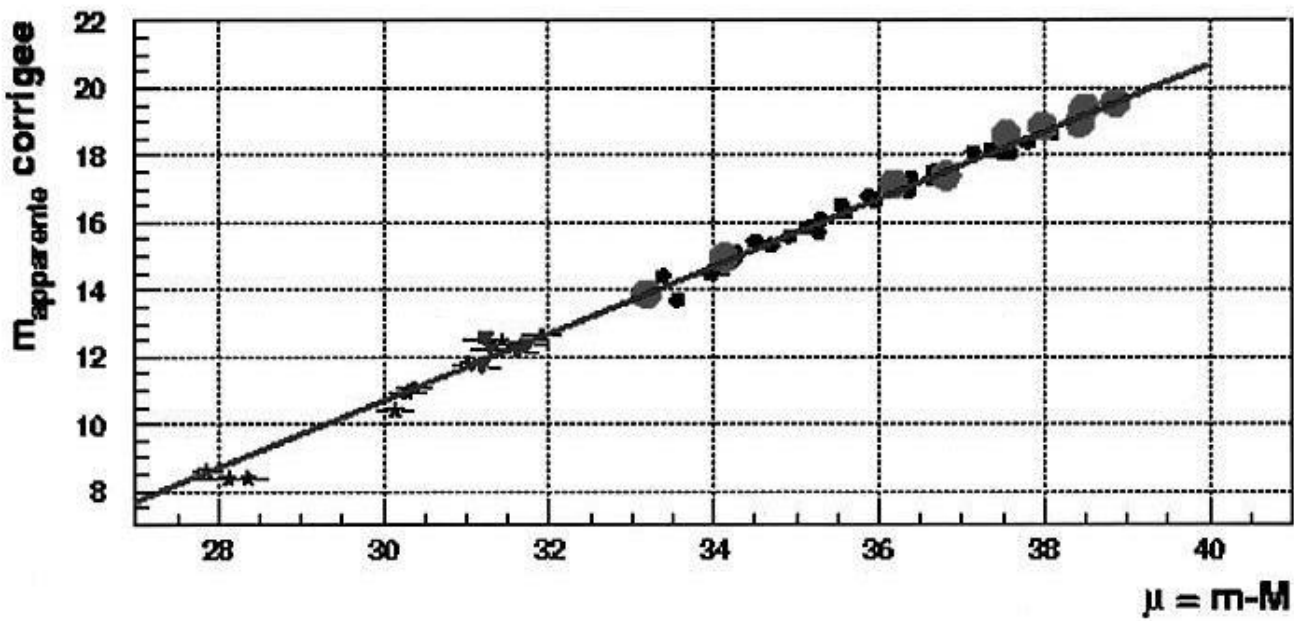
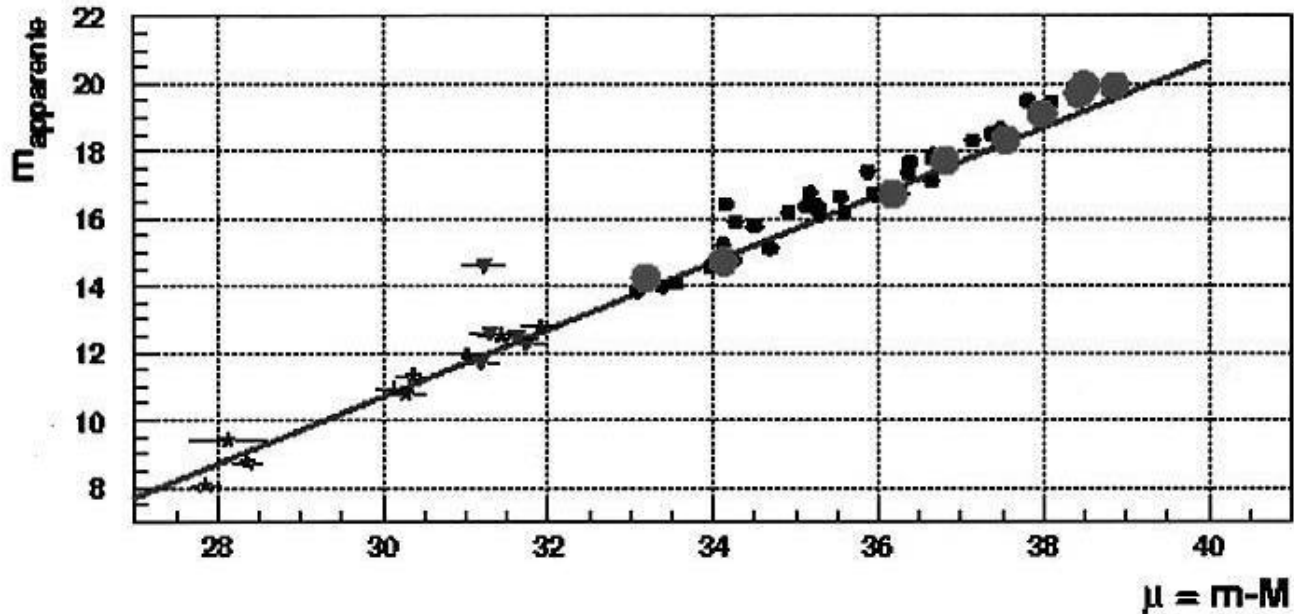
Angular Size Distance:

$$d_\theta(z) \equiv \frac{l}{\theta(z)} = \frac{1}{(1+z) H_o |\Omega_k|^{1/2}} \text{sinn}\left[|\Omega_k|^{1/2} \int_0^z \frac{dz}{(1+z) E(z)}\right]$$

Luminosity Distance:

$$d_L(z) \equiv \sqrt{\frac{L_{bol}}{4\pi f_{bol}(z)}} = \frac{(1+z)}{H_o |\Omega_k|^{1/2}} \text{sinn}\left[|\Omega_k|^{1/2} \int_0^z \frac{dz}{(1+z) E(z)}\right]$$

Where $\text{sinn} \equiv \sinh$ if $\Omega_k > 0$, $\text{sinn} \equiv \sin$ if $\Omega_k < 0$,
and $\text{sinn} \equiv 1$ if $\Omega_k = 1$.



EPM
SN II

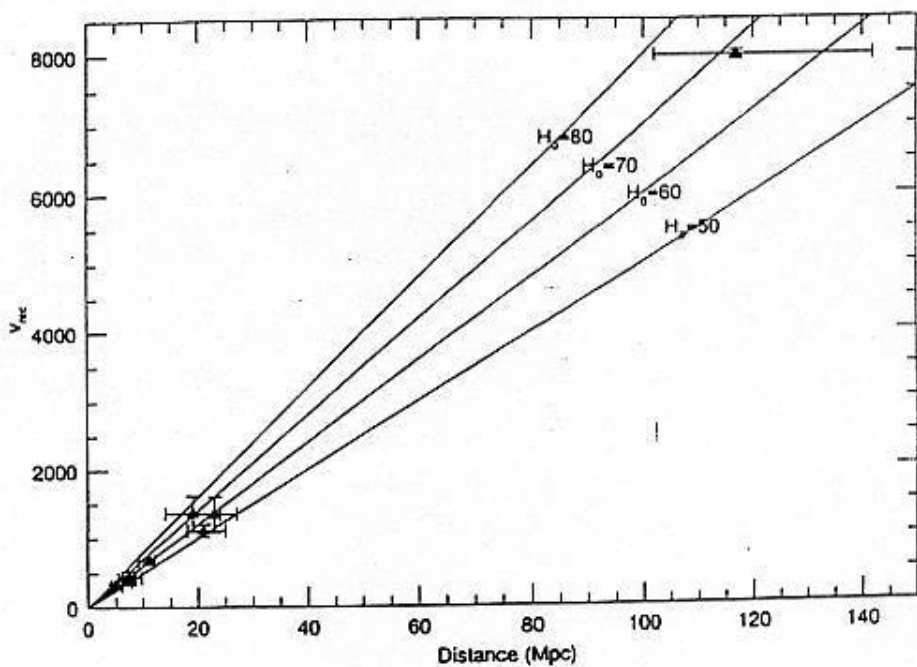


FIG. 13.—The Virgo-corrected velocities for nine galaxies with SN II's are plotted against their distances derived using the Expanding Photosphere Method. Lines for Hubble constants ranging from 50 to $80 \text{ km s}^{-1} \text{ Mpc}^{-1}$ are shown.

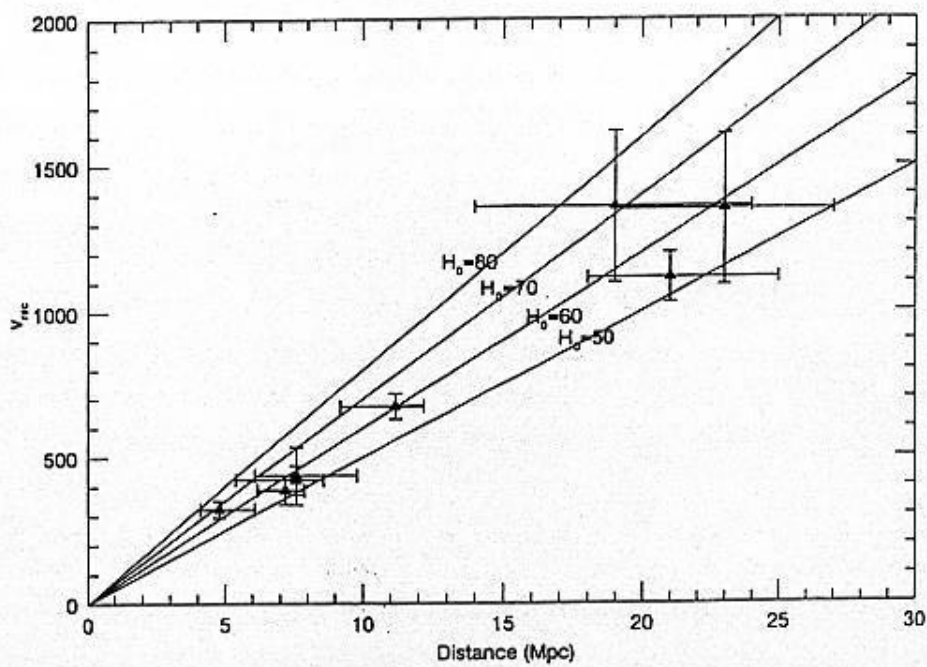
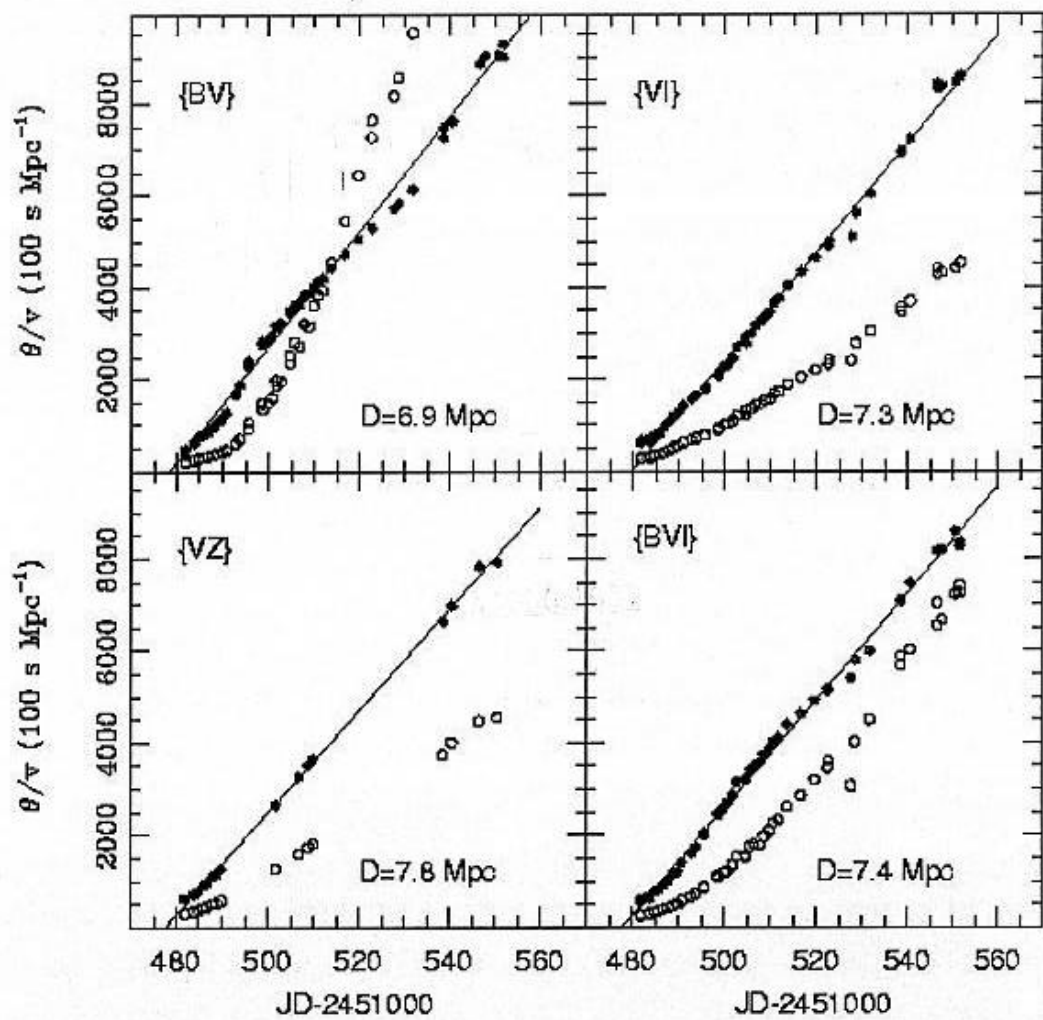


FIG. 12.—The Virgo-corrected velocities for eight galaxies with SN II's (SN 1990ae is excluded) are plotted against their distances derived using the Expanding Photosphere Method. Lines for Hubble constants ranging from 50 to $80 \text{ km s}^{-1} \text{ Mpc}^{-1}$ are shown.

Expanding Photosphere Method

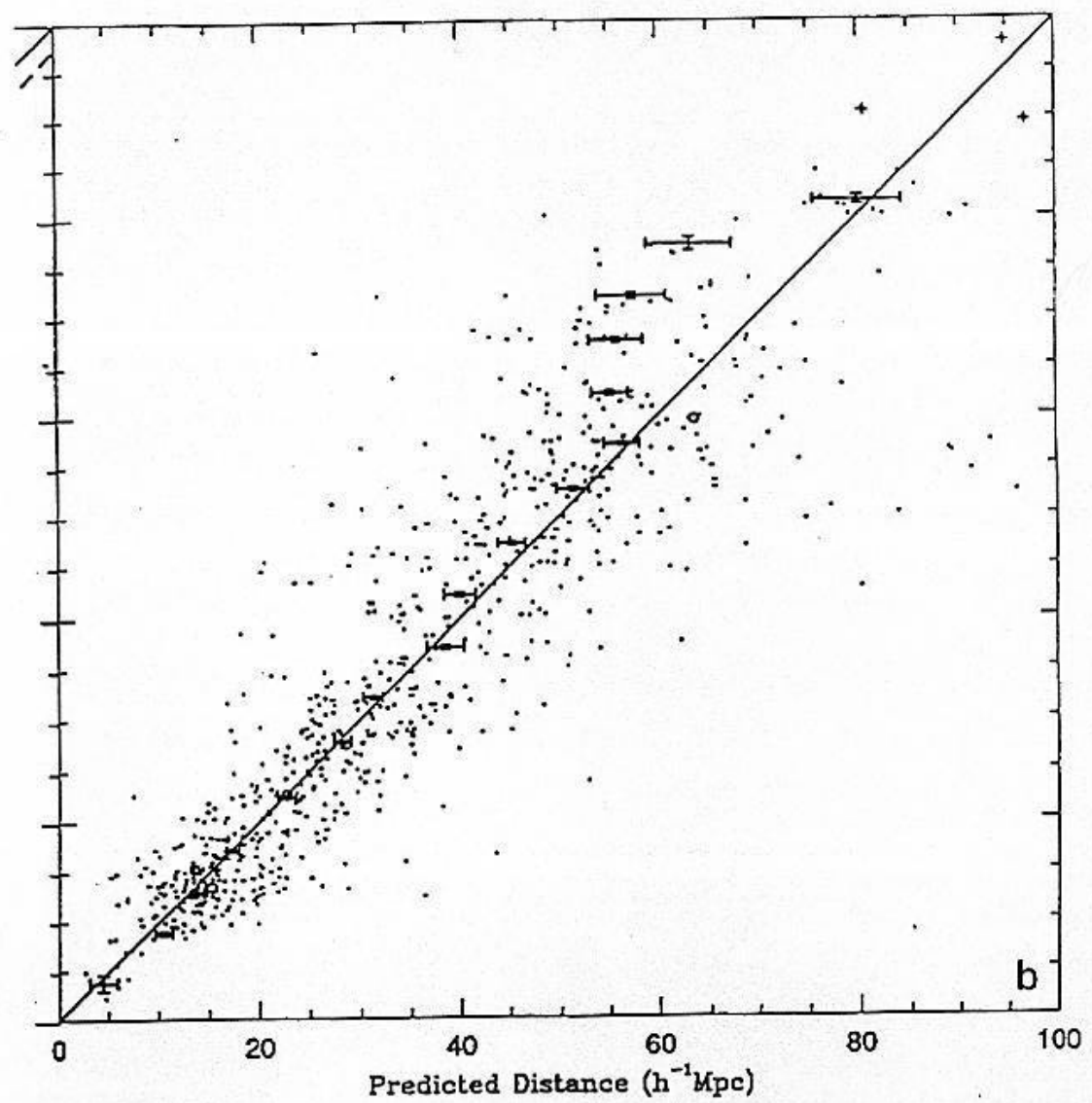
$$\Theta = \frac{R}{D} = \sqrt{\frac{f_v}{\xi \pi B_v(T)}} ; R = v \cdot (t - t_0) + R_0$$



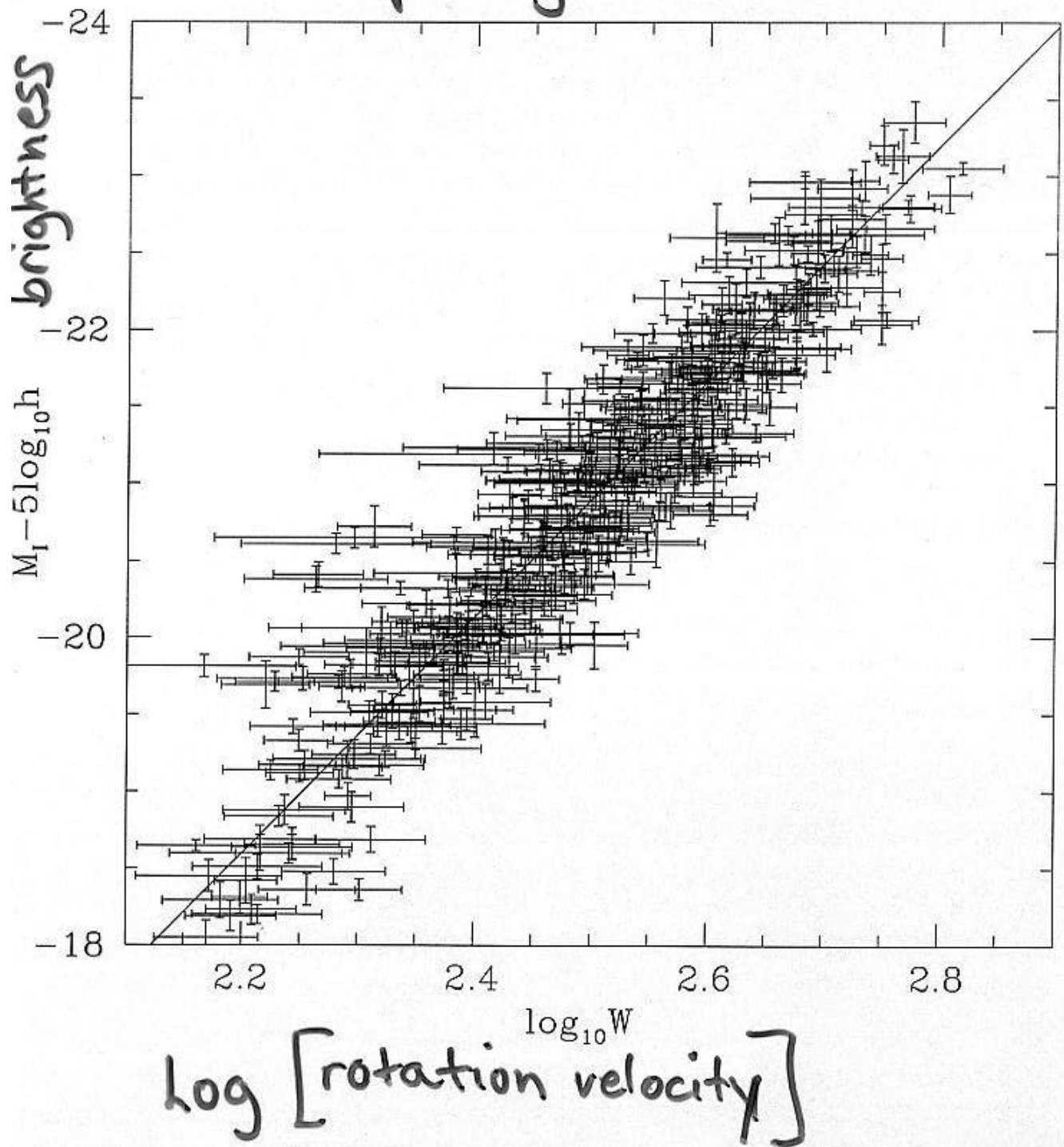
Type II: H atmosphere

Fig. 13.— θ/v as a function of time for filter subsets $\{BV, VI, VZ, BVI\}$. Open dots show θ/v uncorrected for dilution factor while filled dots show the parameter corrected with the factors computed by E96. In theory, this quantity should increase linearly with time and the slope of the relation gives the distance (Appendix A). The small departures of these points from the ridge lines demonstrate the good performance of the dilution factors at different times over a broad wavelength range.

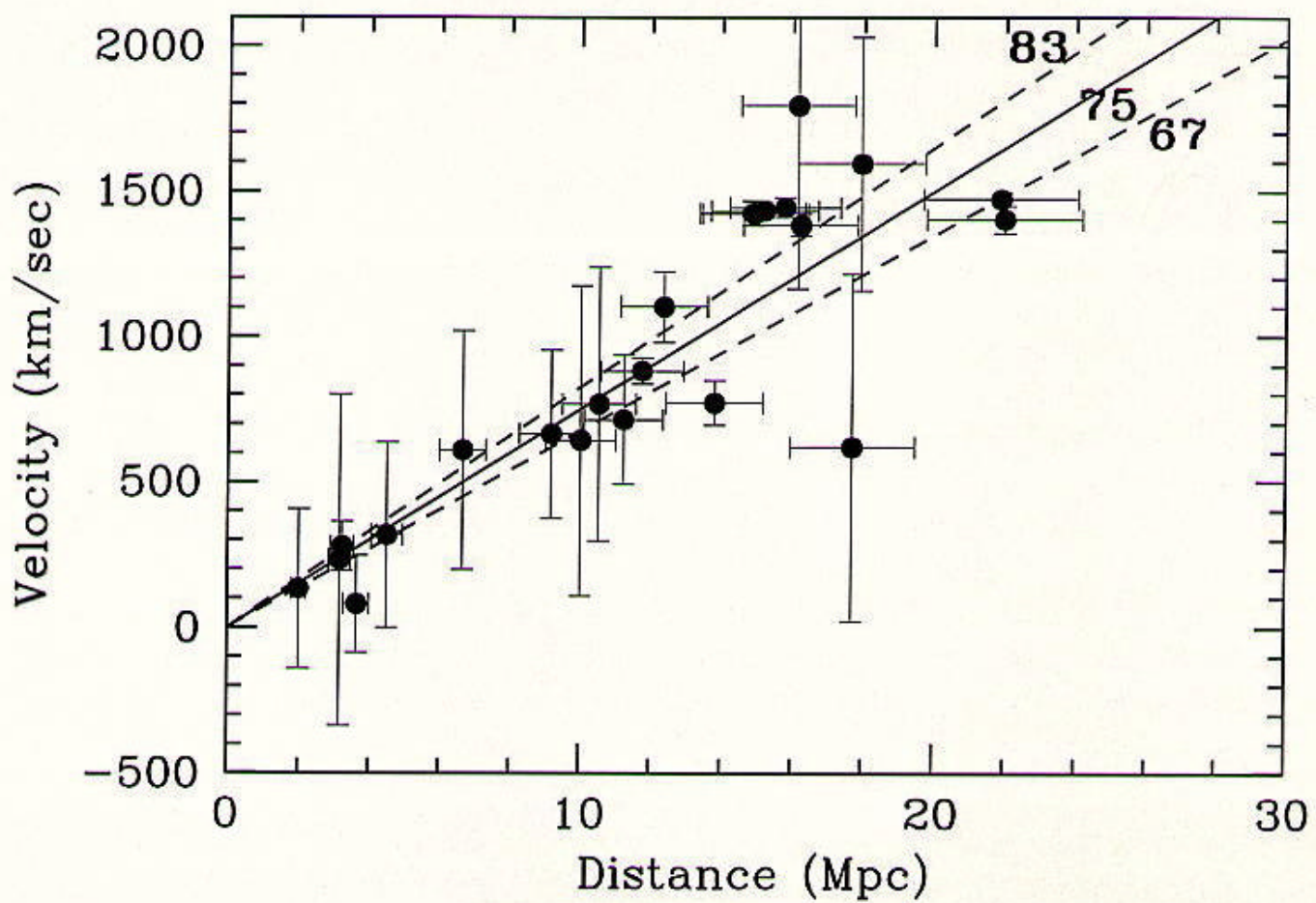
Tully-Fisher Relation



Tully-Fisher Relation
— spiral galaxies



Hubble Diagram for Cepheids (flow-corrected)



good to $\sim 10\%$ in distance

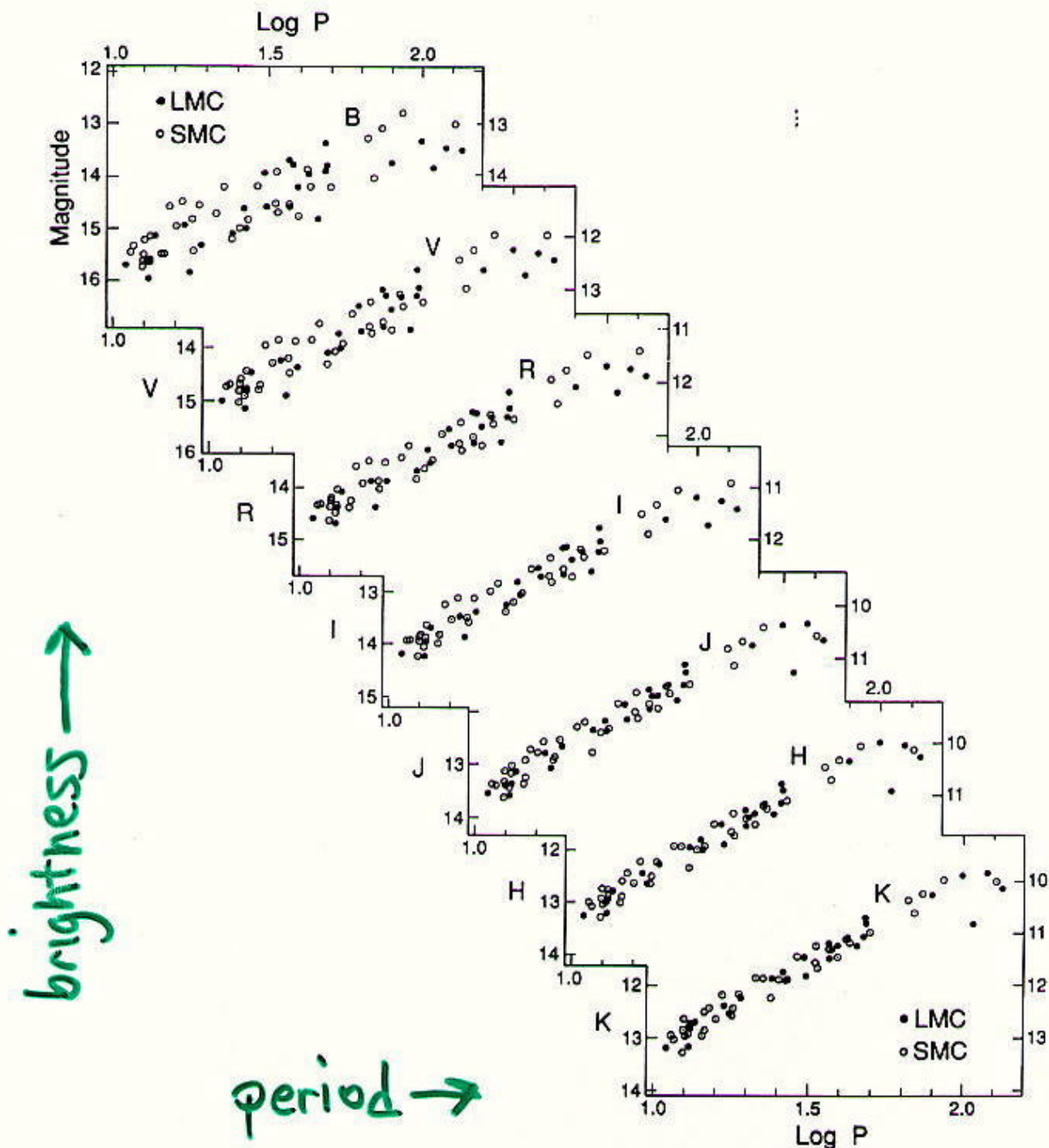
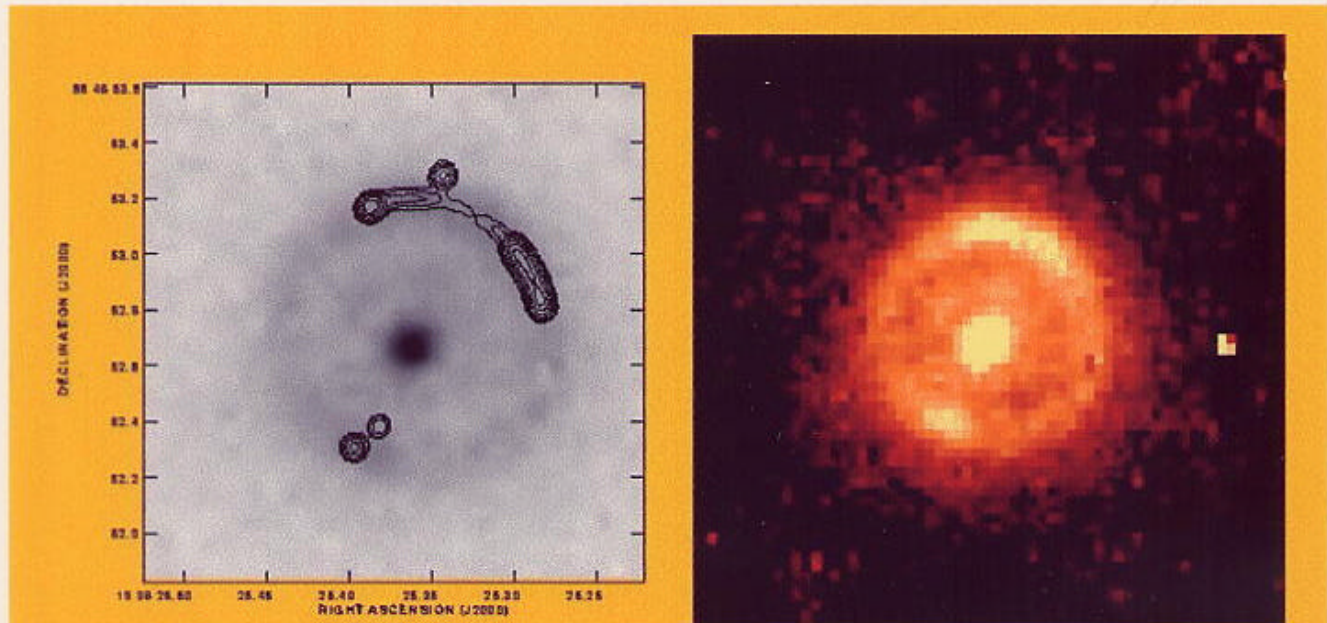


FIG. 4—Magellanic Cloud Cepheid period-luminosity relations at seven wavelengths, from the blue to the near-infrared, constructed from a self-consistent data set (Freedman & Madore 1992). LMC Cepheids are shown as filled circles; SMC data, shifted to the LMC modulus, are shown as open circles. Note the decreased width and the increased slope of the relations as longer and longer wavelengths are considered.

data, applying it first to single-epoch observations of Cepheids in IC 1613 and later refining it and expanding its application to data obtained for M 31, M 33, and NGC 300 as cited below. For a detailed discussion of the technique and its implementation the interested reader is

referred to those papers. Briefly stated, one determines differential apparent moduli, scaled against the corresponding LMC PL relations. By assuming that all difference as a function of inverse wavelength can be attributed to selective absorption, fitting an interstellar extinction



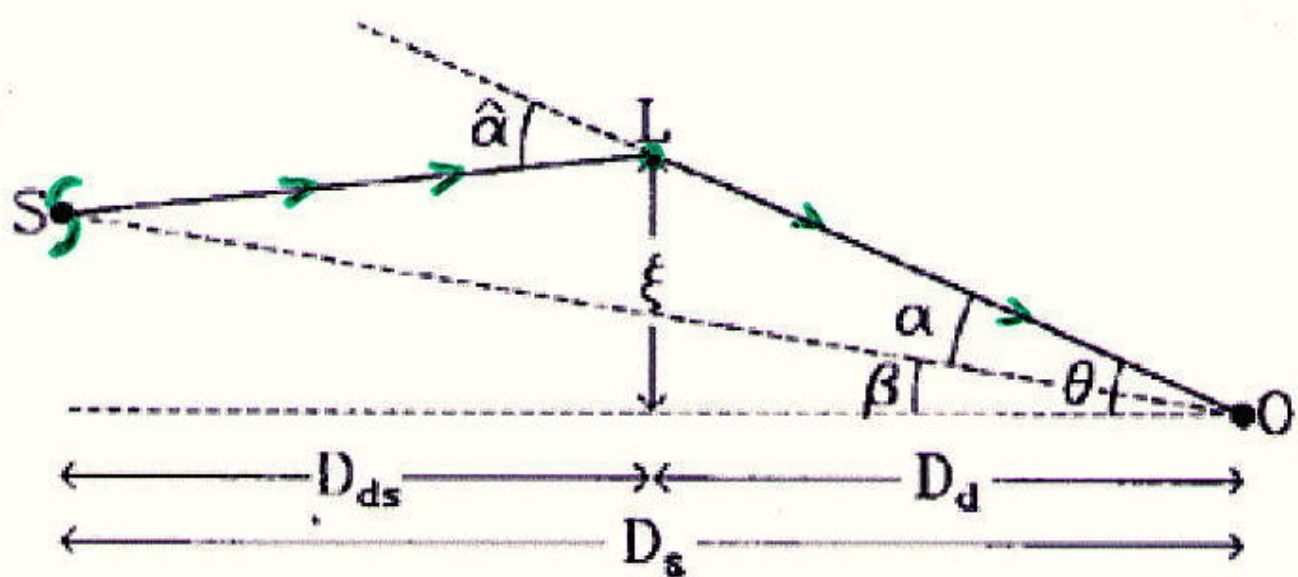
The gravitational lens JVAS B1938+666

Left: HST/NICMOS greyscale with MERLIN radio contours

Right: Colour image of the HST/NICMOS image

Lens mass model biggest uncertainty

Strong Gravitational Lensing Time Delays



$$\tau = \tau_{\text{geom}} + \tau_{\text{grav}}$$

$$= \frac{1+z_s}{c} \frac{D_L D_S}{D_{LS}} \left(\frac{1}{2} (\vec{\theta} - \vec{\beta})^2 - \psi(\theta) \right)$$

\uparrow
 potential
 of lens

Sunyaev-Zeldovich Effect + X-ray

$\Delta T \propto n_{\text{eff}} \rightarrow$ inverse Compton scattering

$$f_X \propto n_{\text{eff}}^2/d^2 \propto \Delta T^2/d^3 \theta$$

CL 0016+16 z=0.54 BIMA

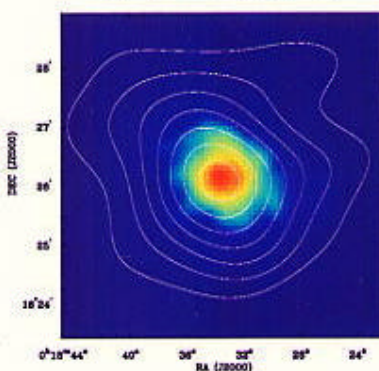
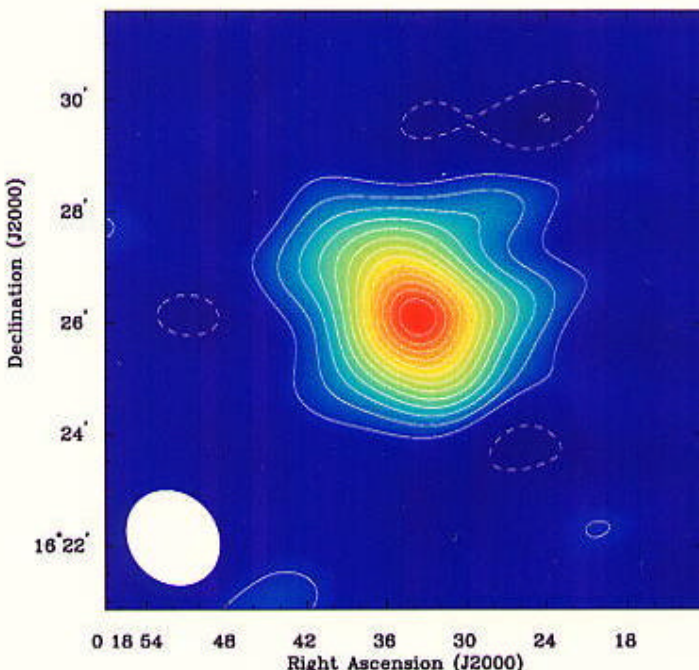
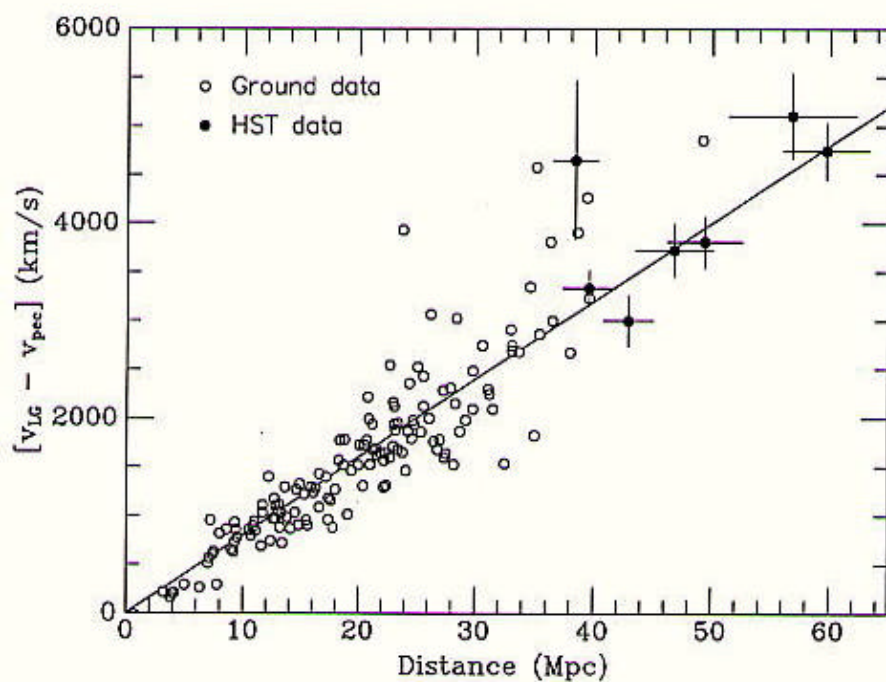


Figure 2. S-Z and X-ray images of the cluster CL 0016+16. The S-Z image (false color) of the cluster, obtained with the BIMA array, is shown in the upper frame. In the lower frame, contours of the S-Z effect in the cluster are superposed on the *ROSAT* X-ray (false color) image (from Carlstrom *et al.* 1999).

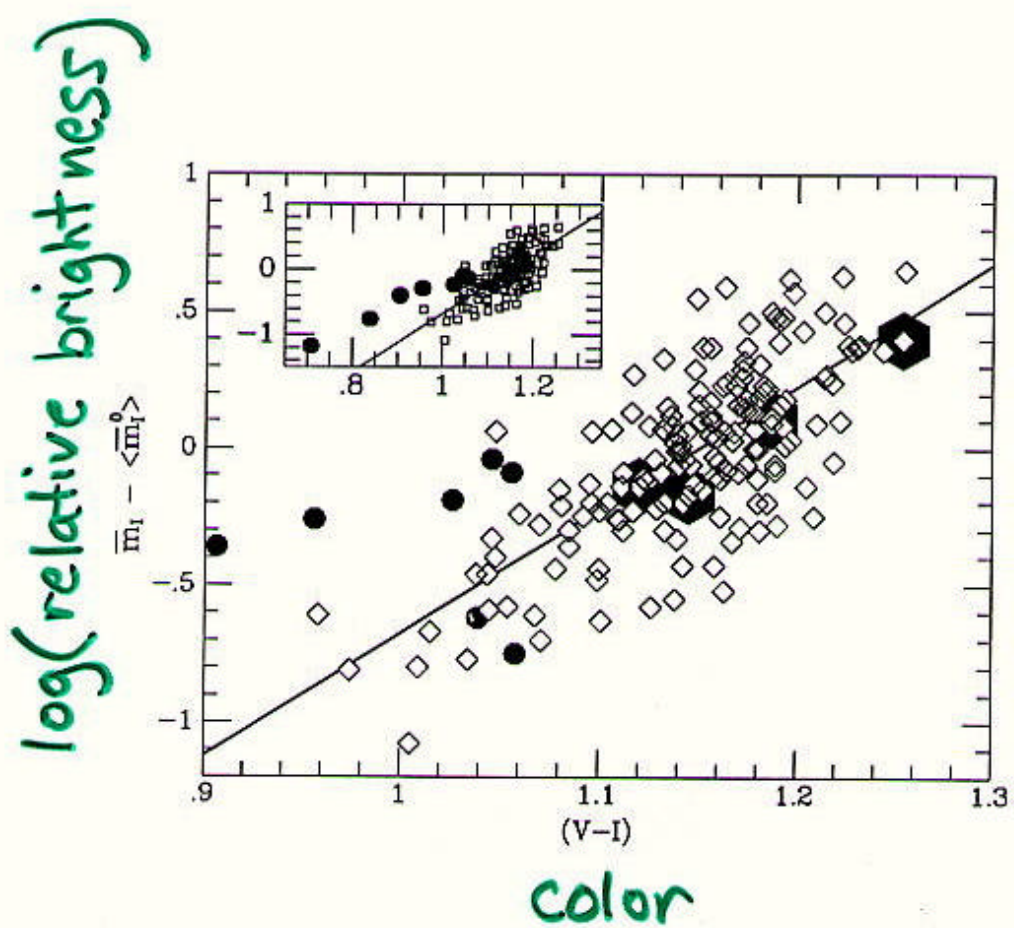
Surface Brightness Fluctuations

redshift ↑



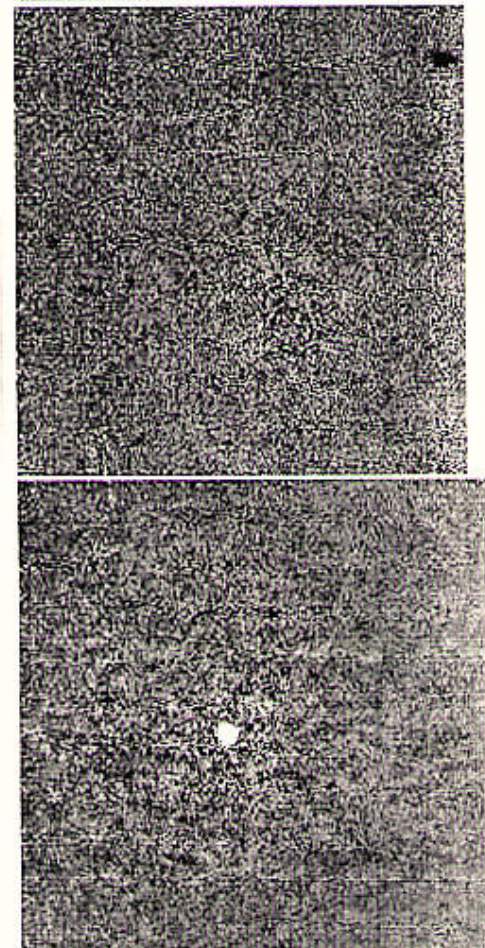
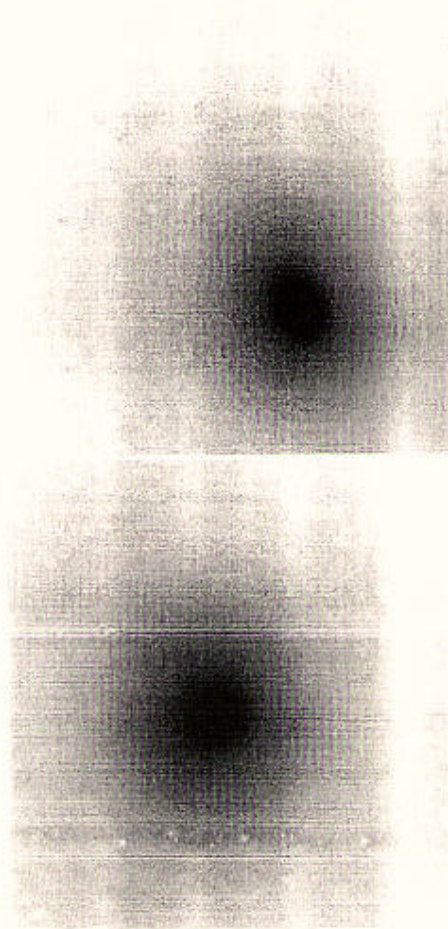
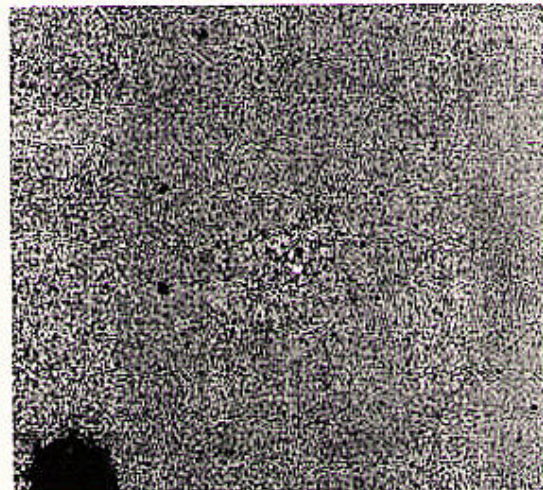
distance →

Surface Brightness Fluctuations

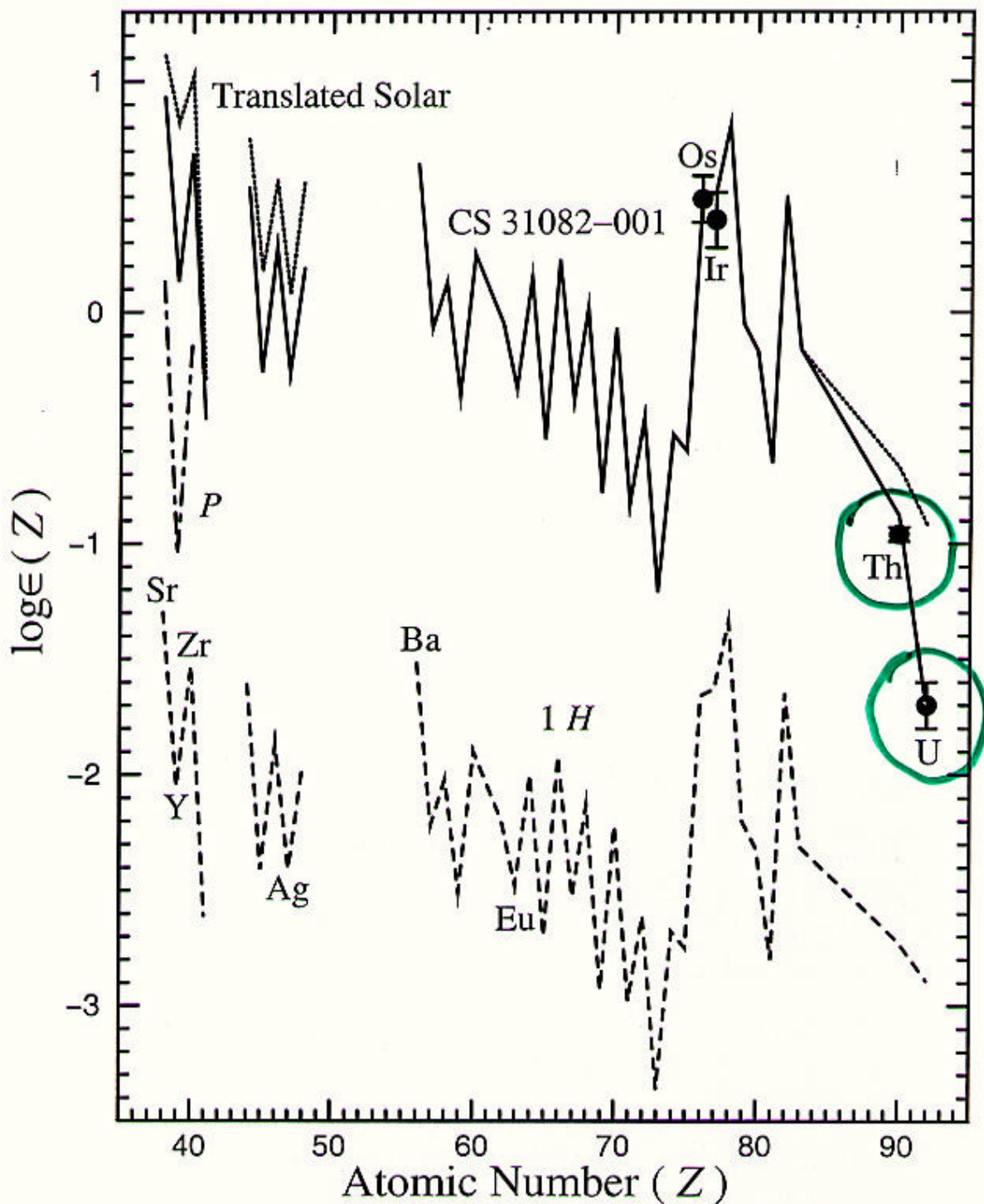


Surface Brightness Fluctuations

galaxy smooth subtraction

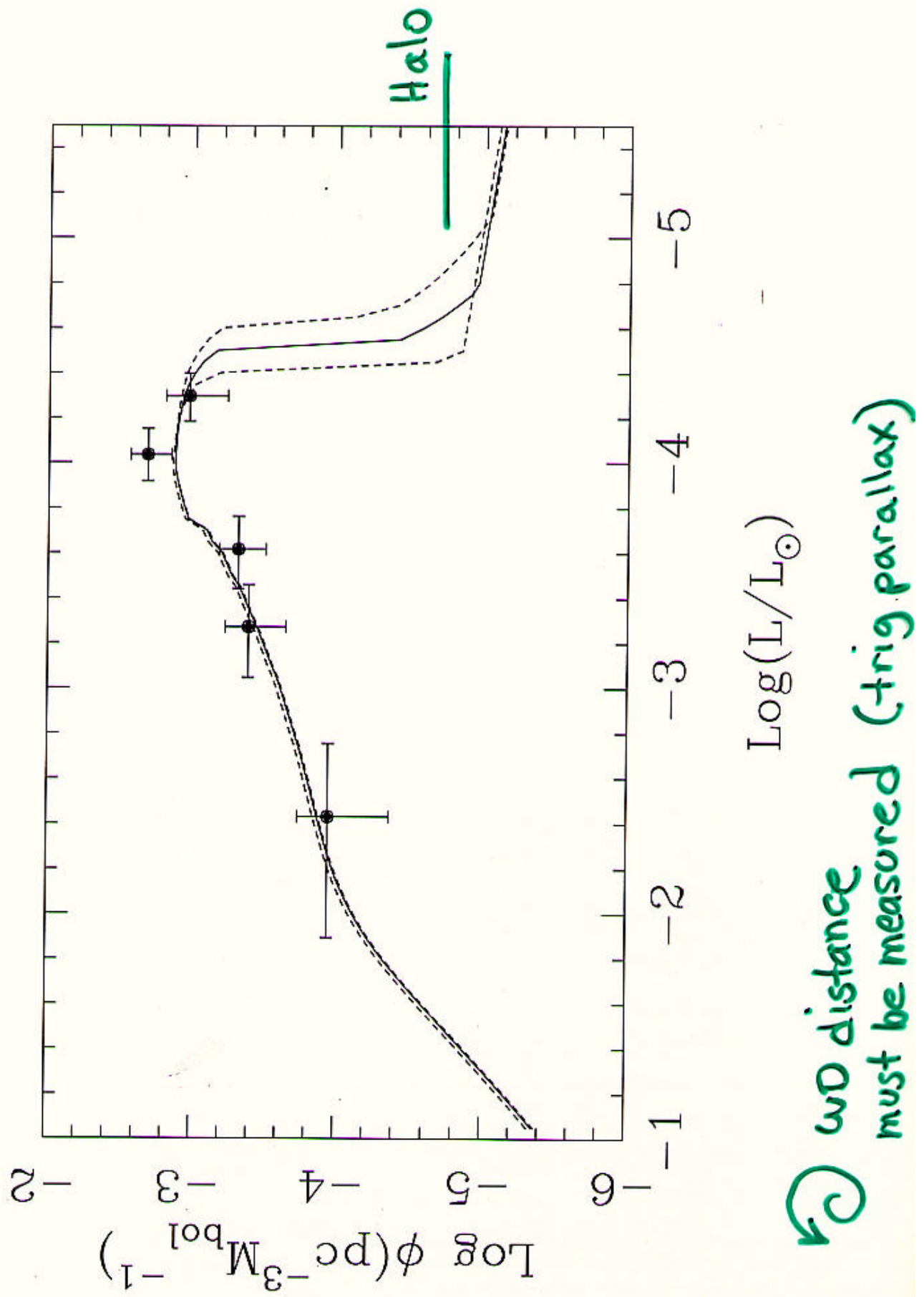


$$\frac{^{232}\text{Th}}{^{232}\text{Th}_0} = e^{-t/20.3 \text{ Gyr}}$$

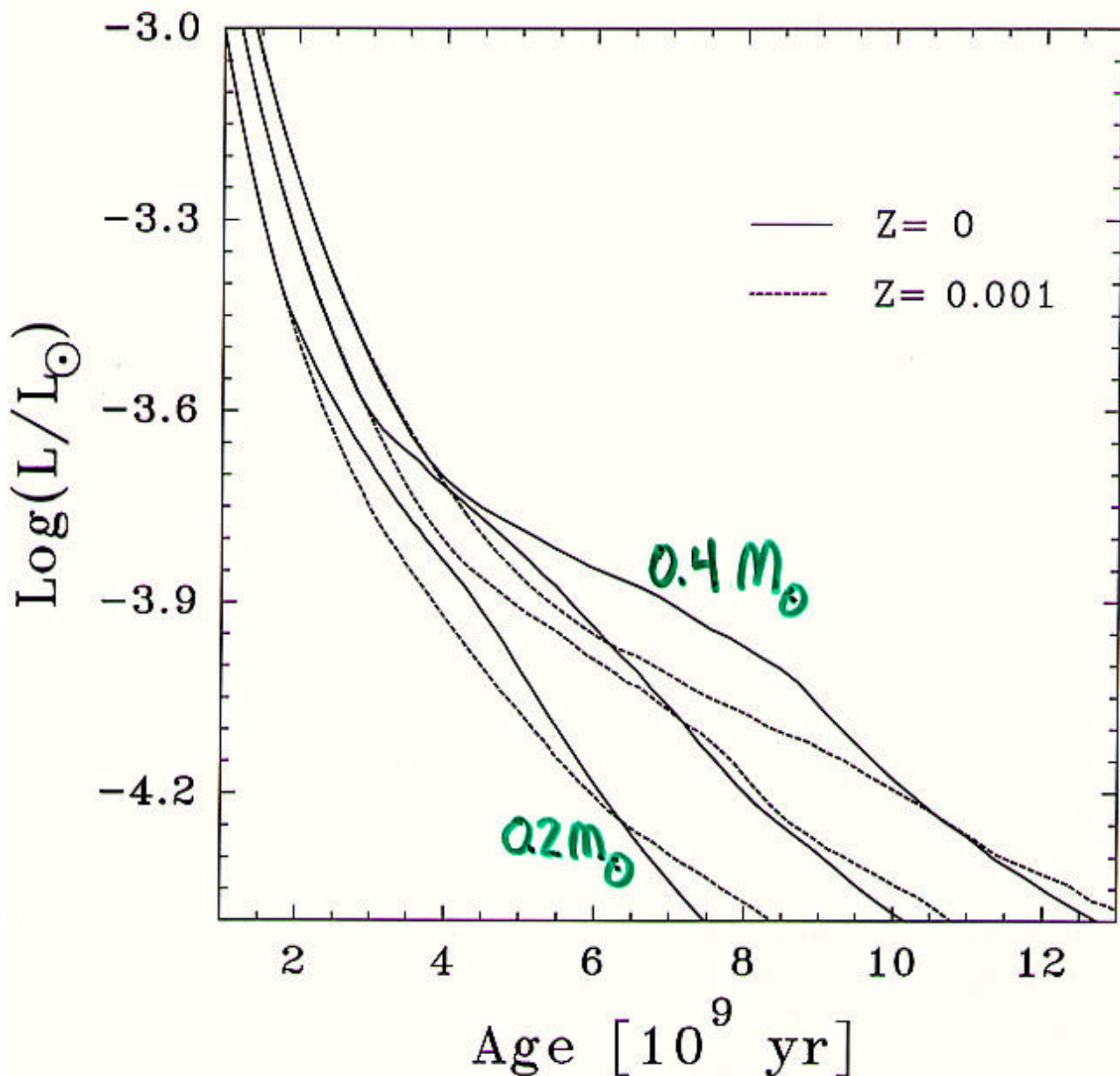


uncertain by ± 4 Gyr

Disk WD's



WD cooling curves



Main Sequence Fitting

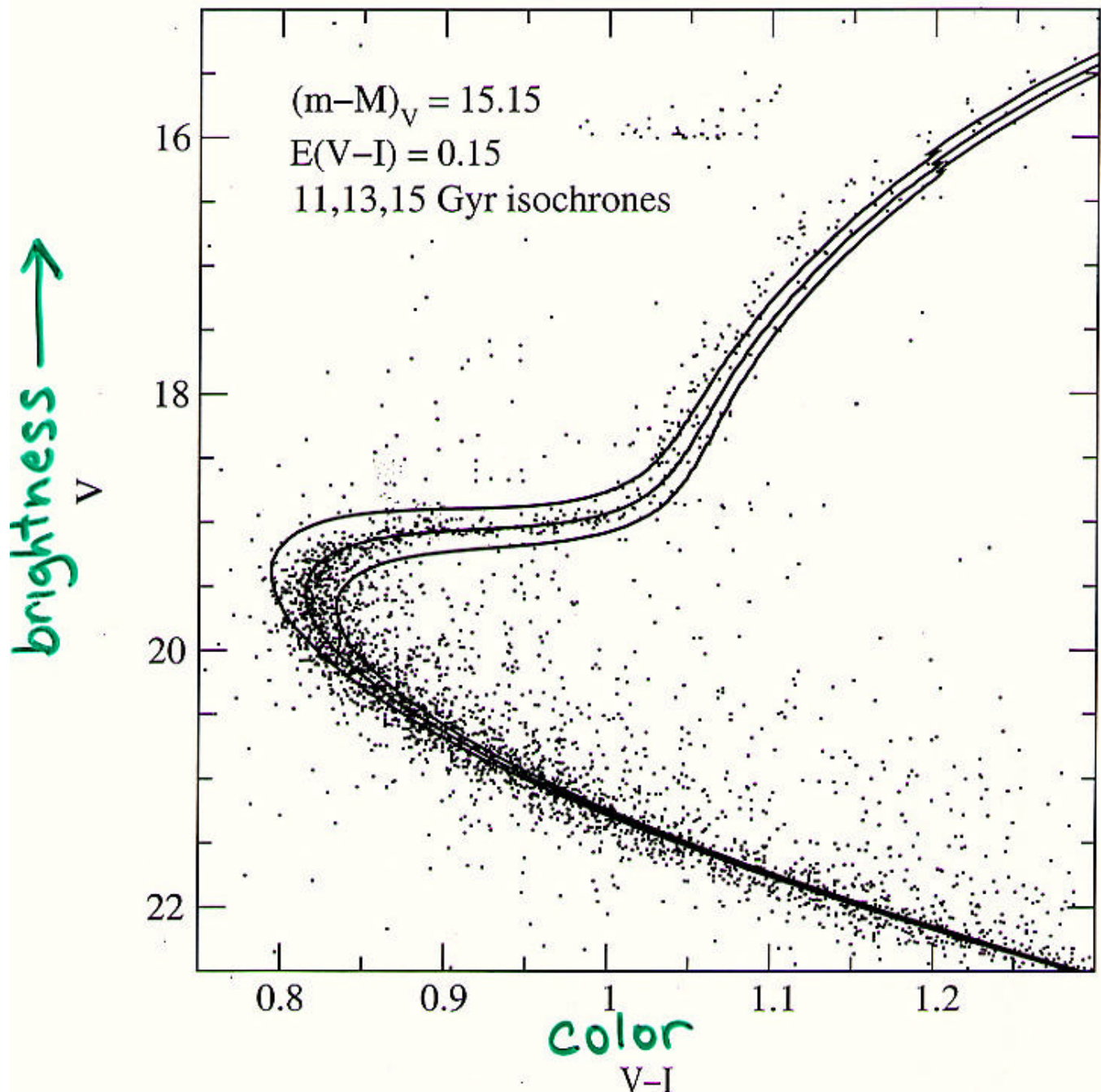


Fig. 7.— The fit of the $[Fe/H] = -0.85$, $[\alpha/Fe] = +0.4$ isochrones to the data.

⌚ cluster distance must be known/fit

Main Sequence Fitting

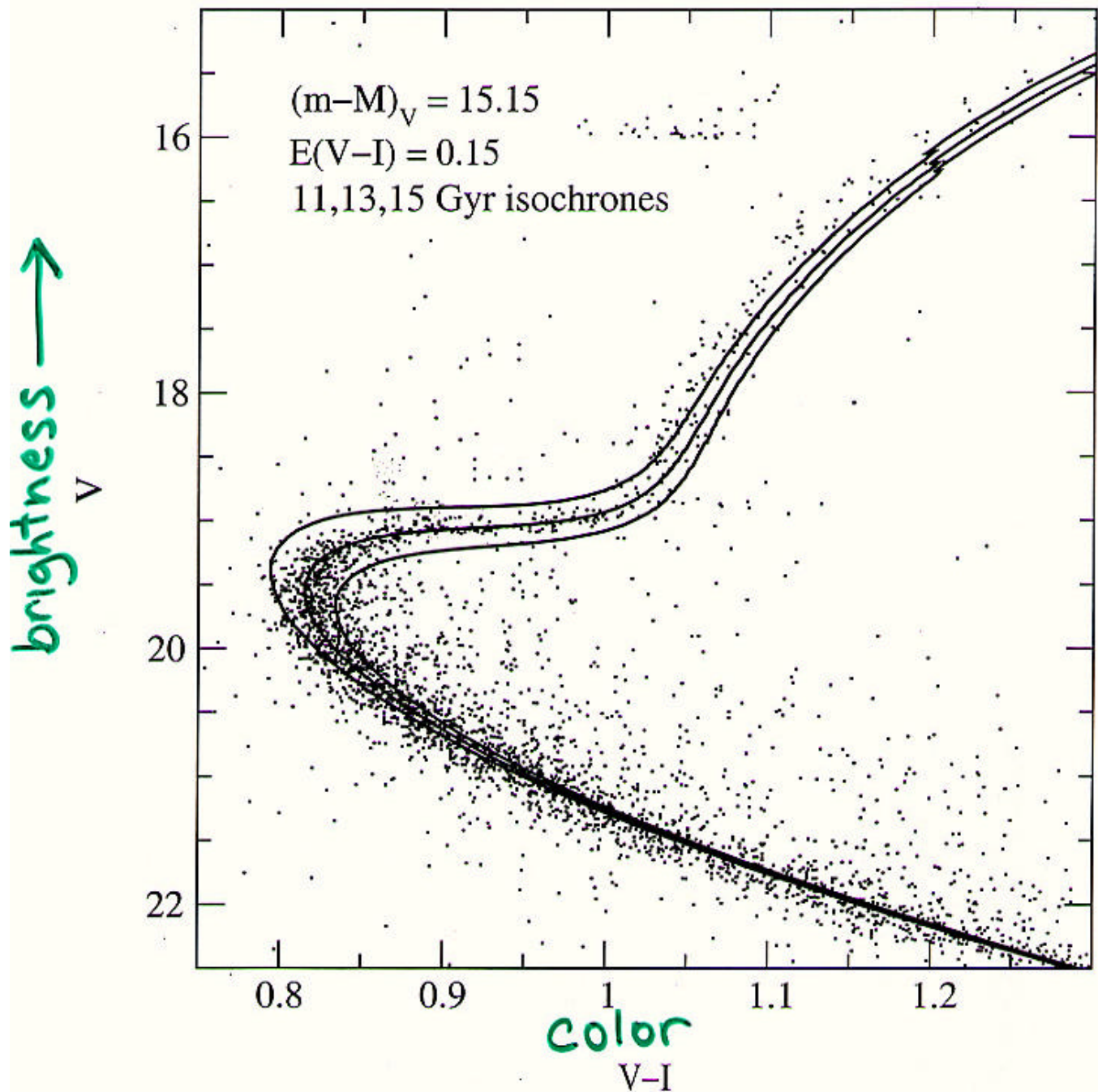
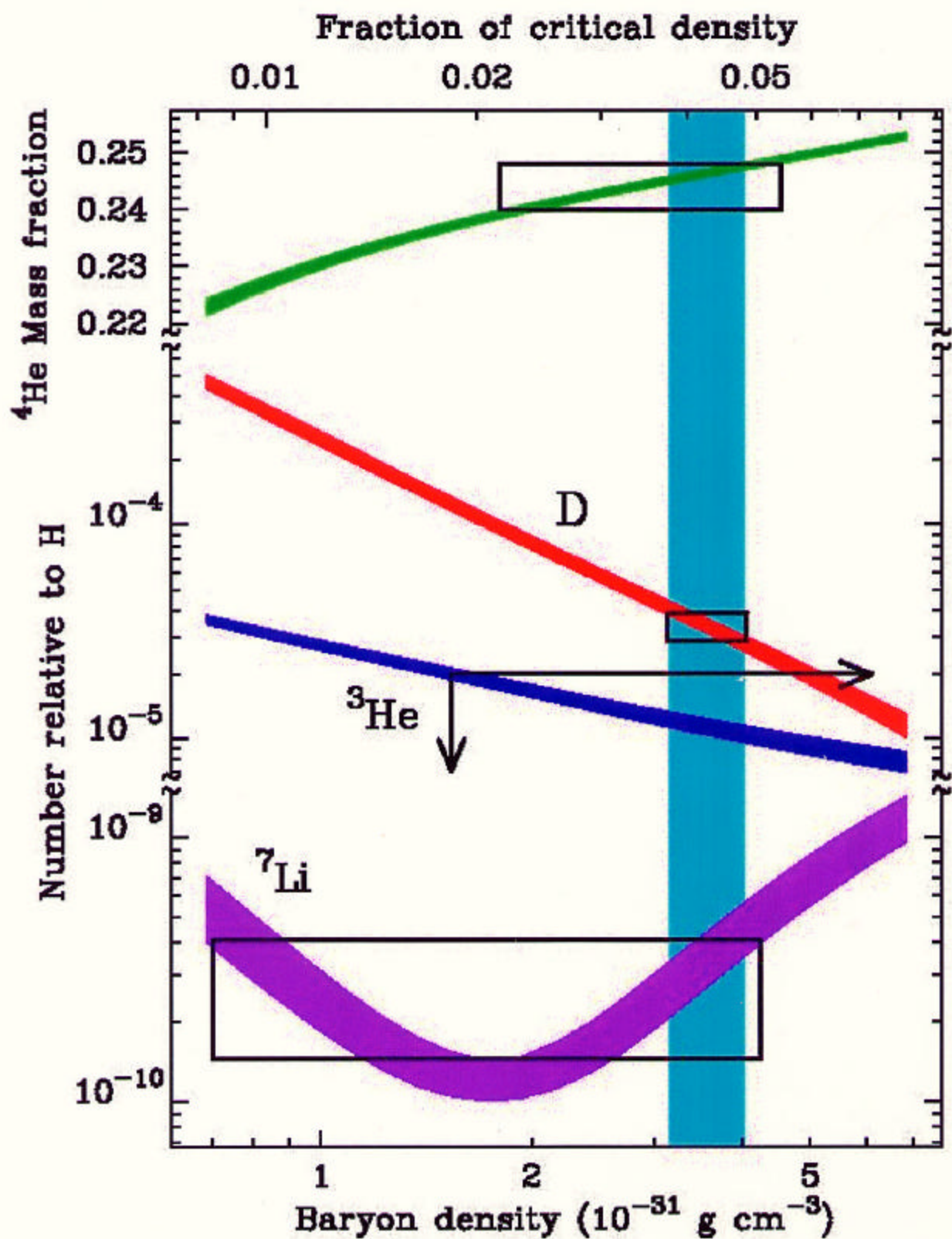
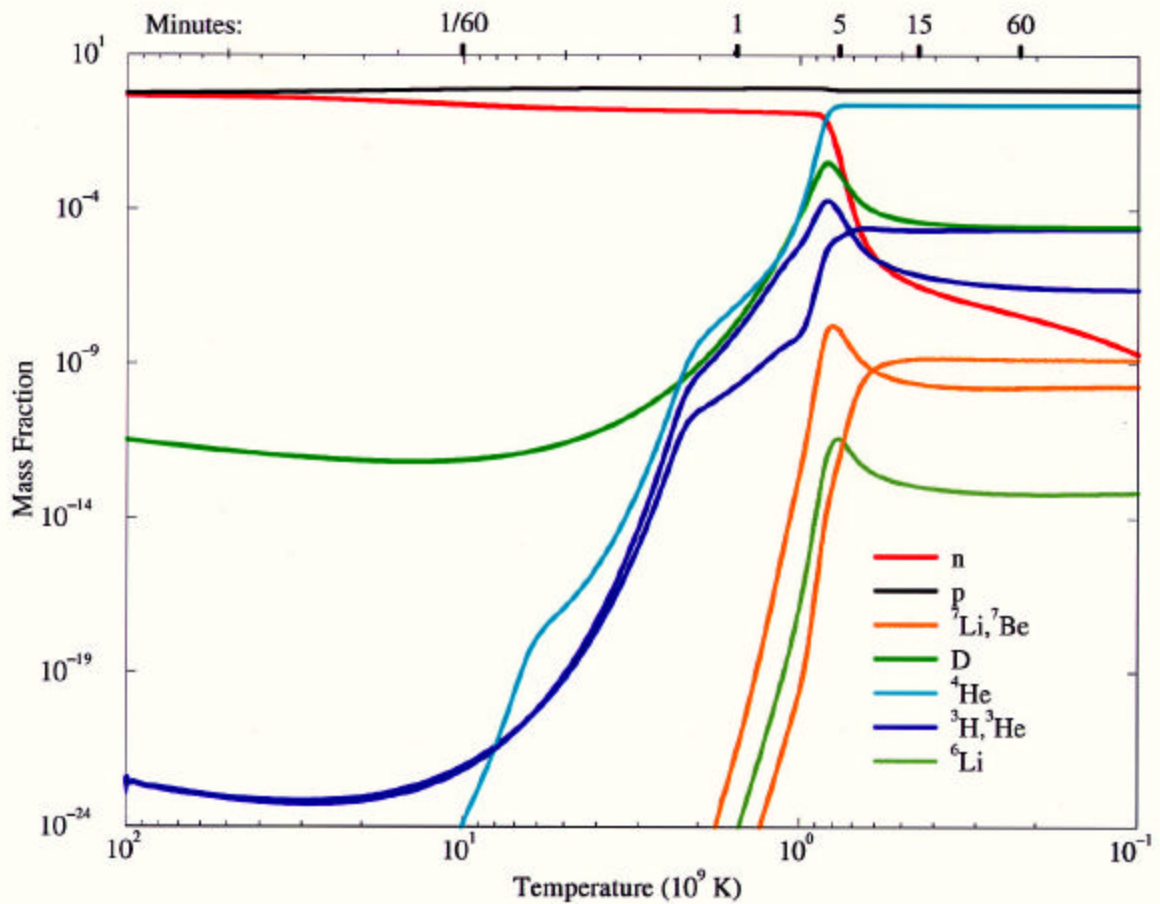
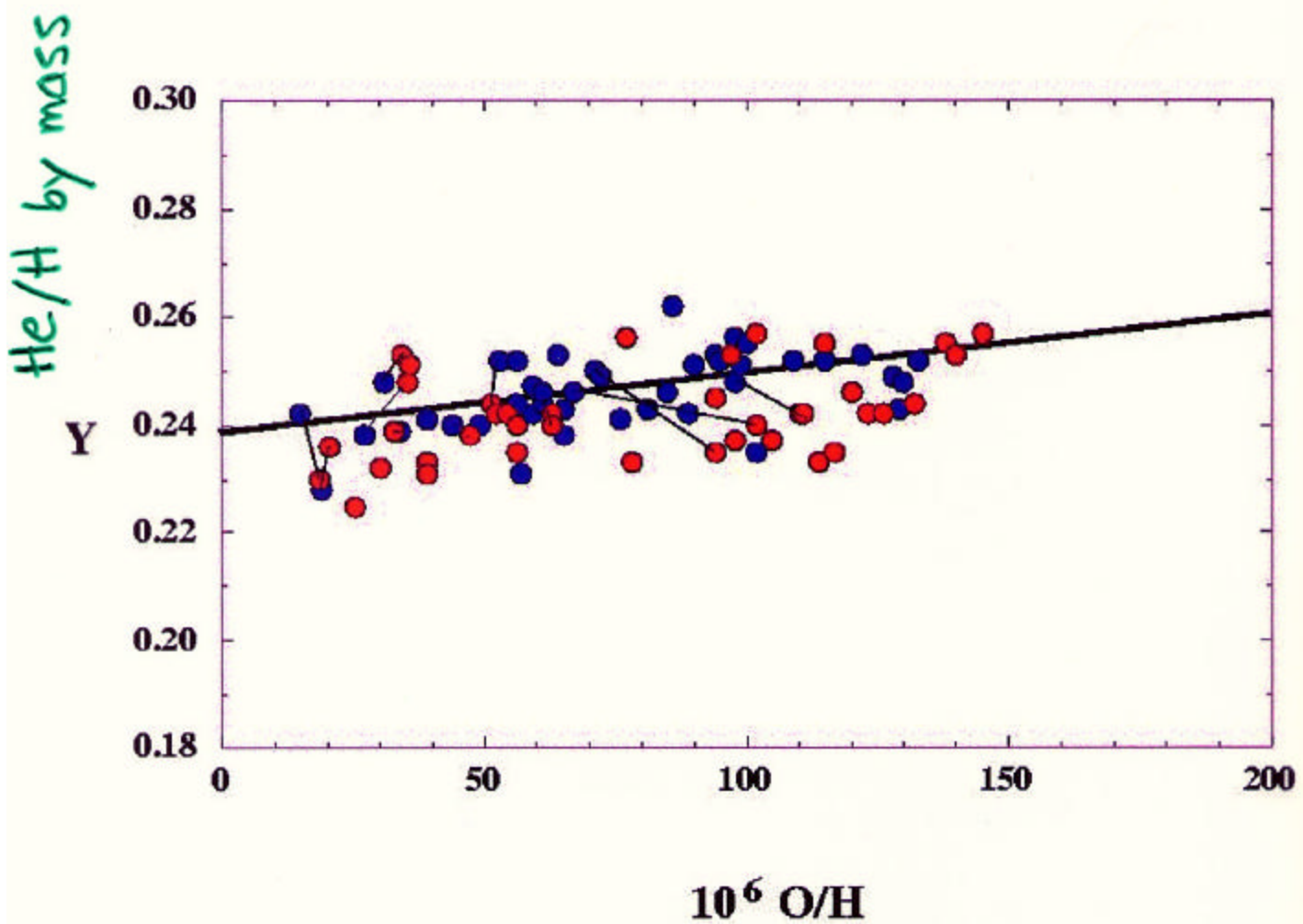


Fig. 7.— The fit of the $[Fe/H] = -0.85$, $[\alpha/Fe] = +0.4$ isochrones to the data.

⌚ cluster distance must be known/fit







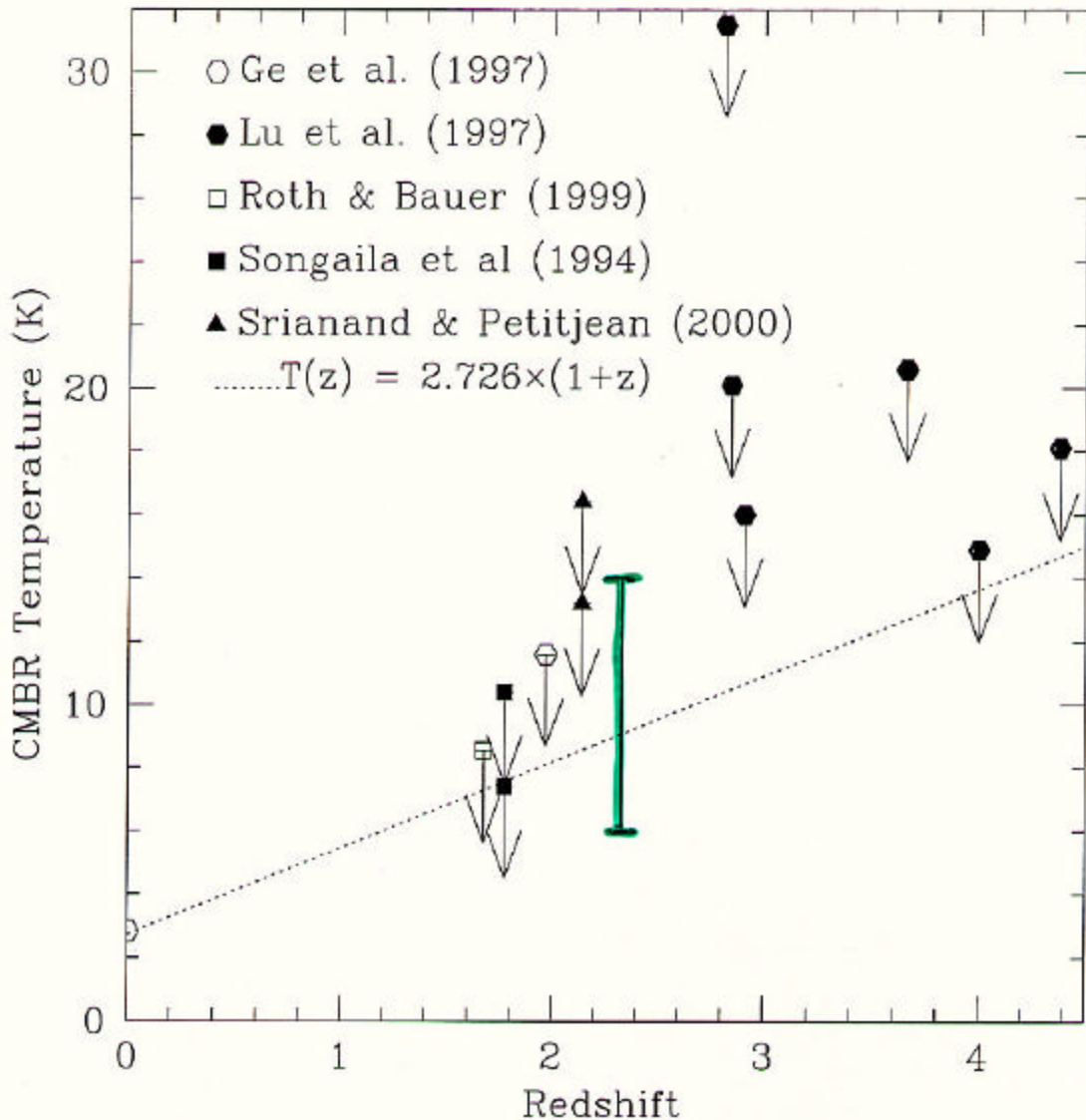


Fig. 5.— Measurements of the Cosmic Microwave Background Radiation temperature at various redshifts: The point at $z = 0$ shows the result of the Cosmic Background Explorer (COBE) determination³, $T_{\text{CMBR}}(0) = 2.726 \pm 0.010$ K. Upper limits are previous measurements^{6,8,9,10} using the same techniques as in this paper. We also include our two new unpublished upper limits at $z = 2.1394$ along the line of sight toward Tololo 1037-270. The measurement from this work, $6.0 < T_{\text{CMBR}} < 14.0$ K at $z = 2.33771$, is indicated by a vertical bar. The dashed line is the prediction from the Hot Big Bang, $T_{\text{CMBR}}(z) = T_{\text{CMBR}}(0) \times (1 + z)$.

neutral C fine-structure

- 16 -

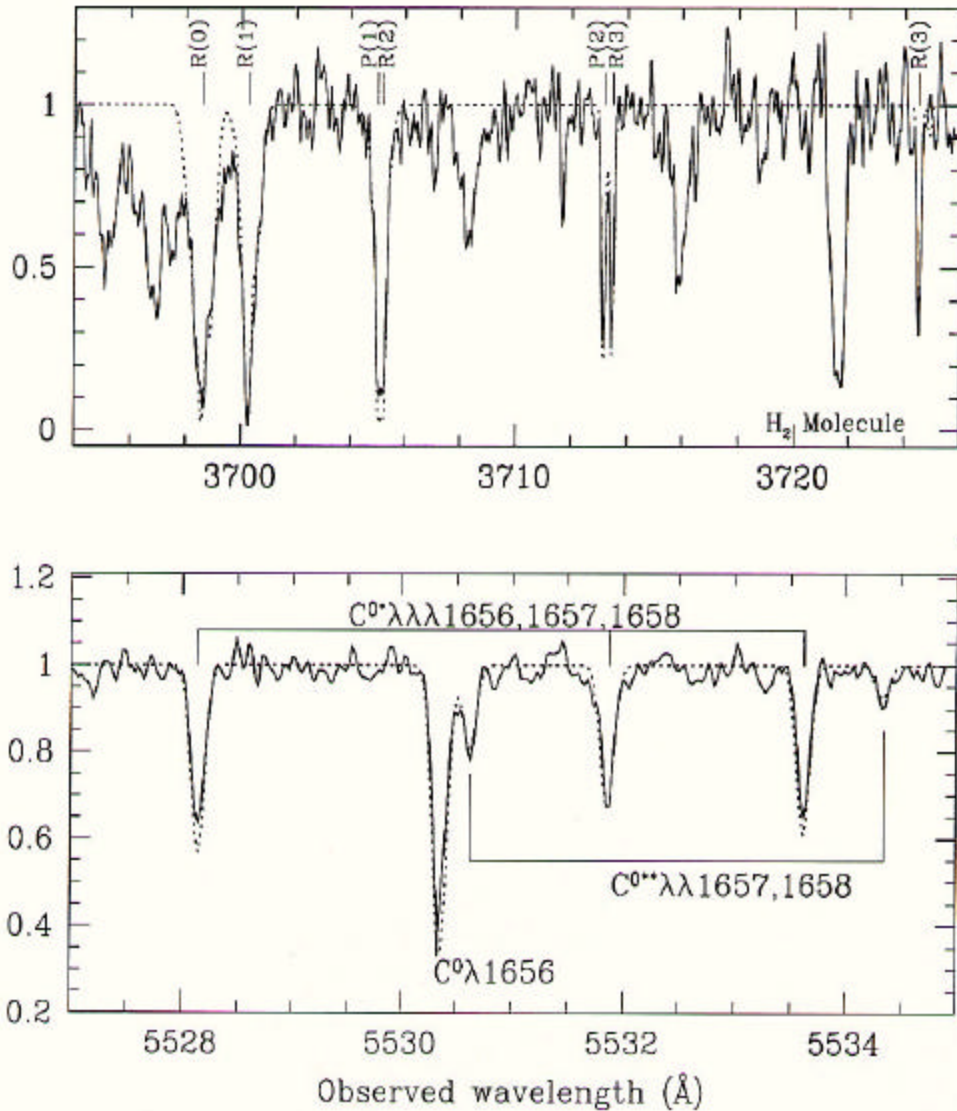
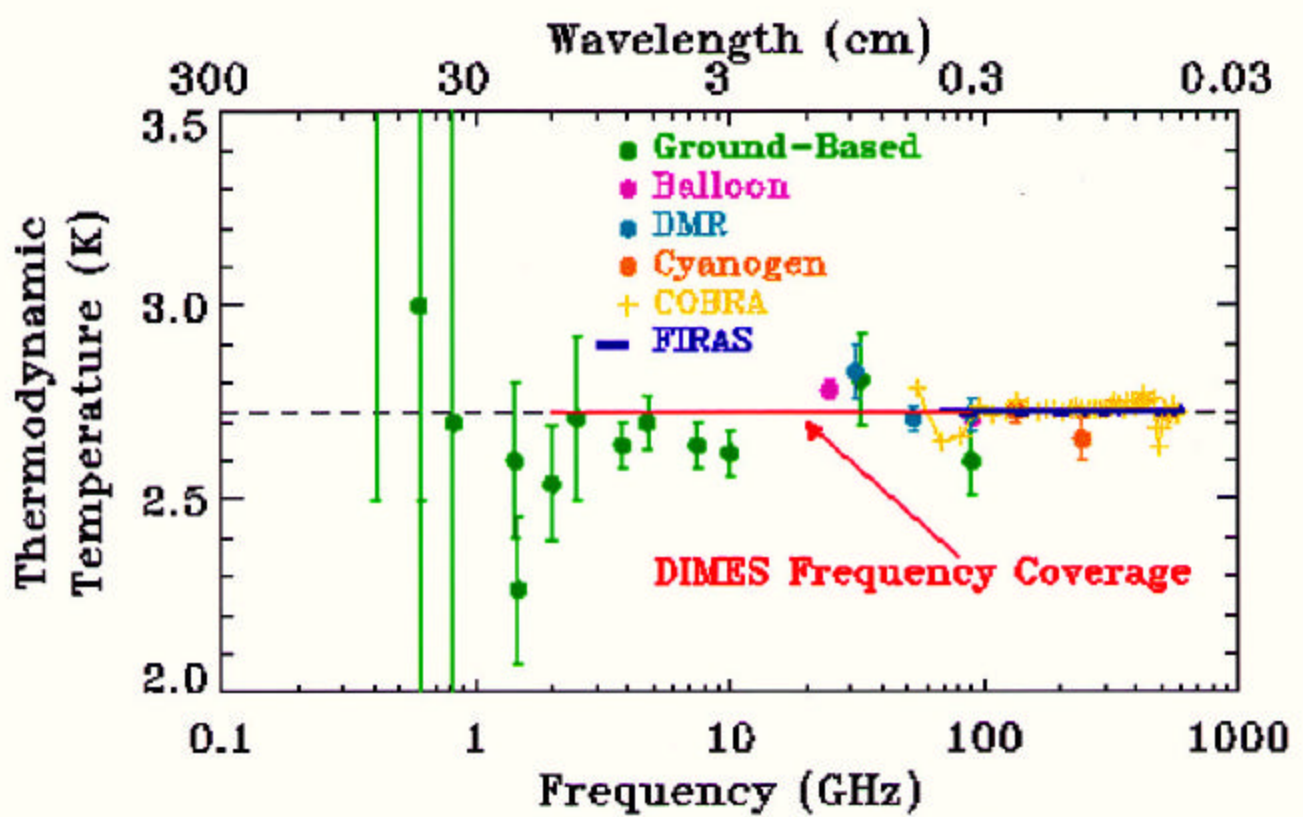
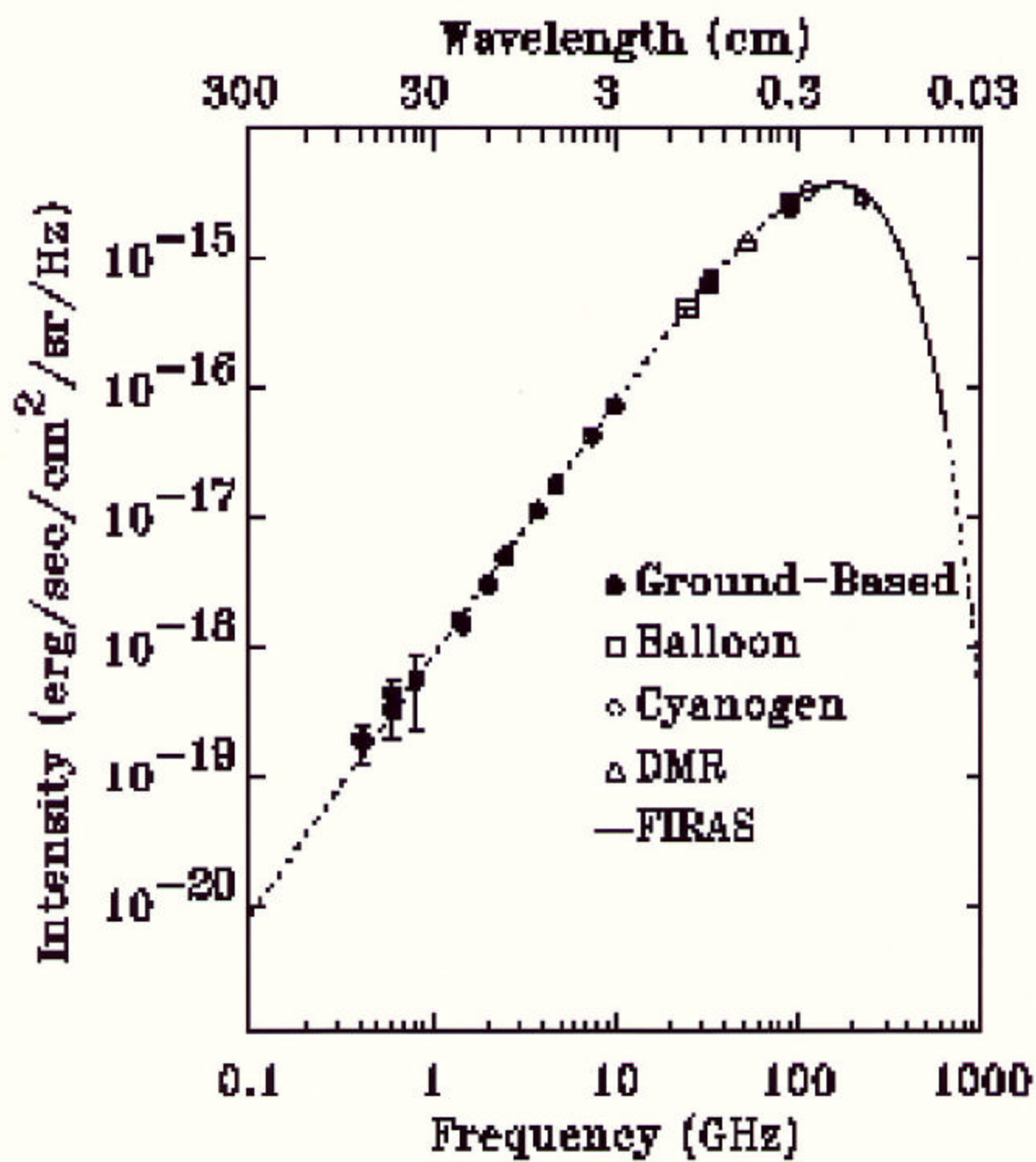
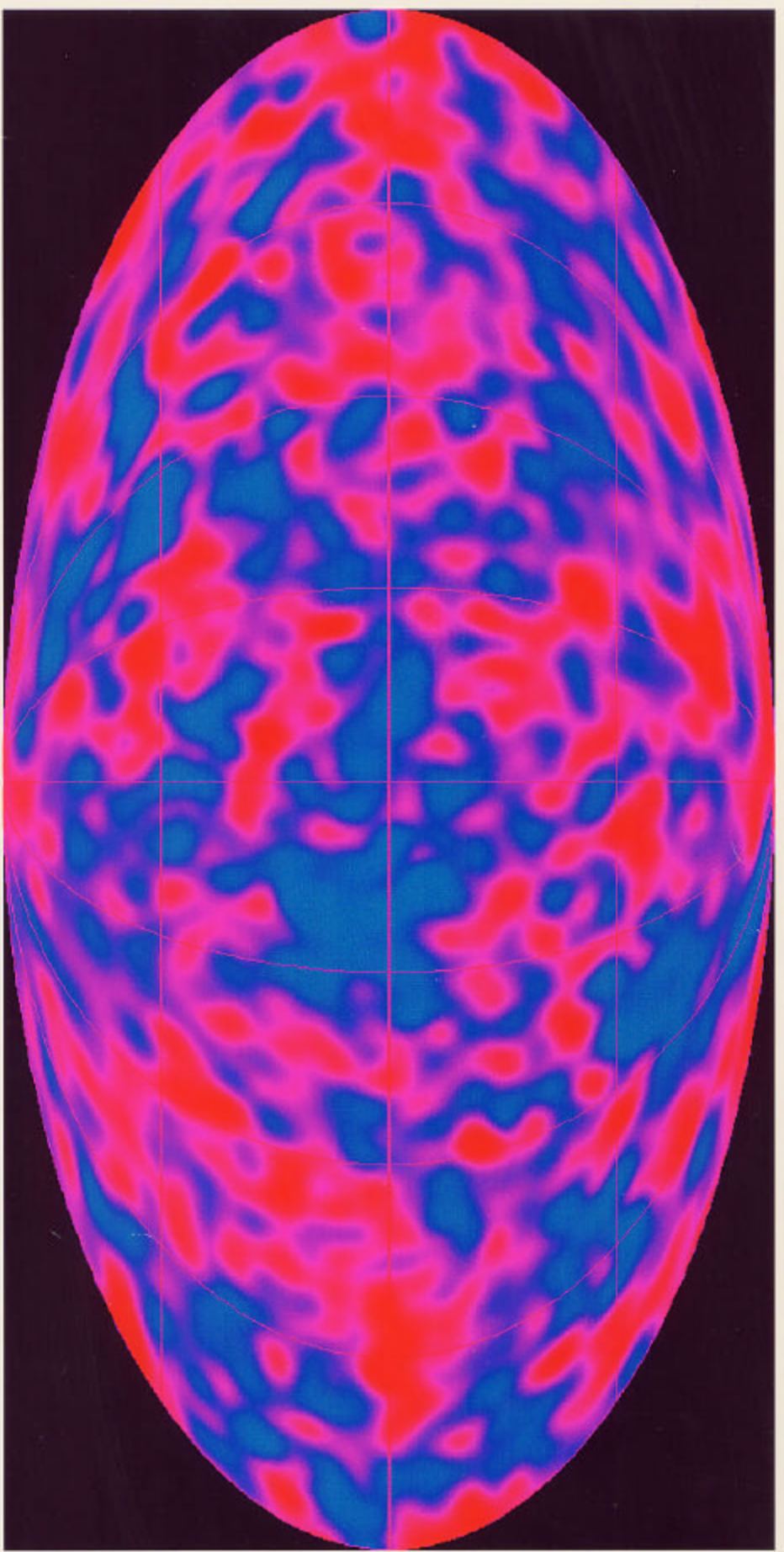


Fig. 1.— A sample of H₂ and C⁰ absorption lines at $z_{\text{abs}} = 2.33771$: Portions of the normalized spectrum of the quasar PKS 1232+0815 taken with the Ultra-violet and Visible Echelle Spectrograph mounted on the 8.2 m KUEYEN telescope of the European Southern Observatory on the Paranal mountain in Chile. *Upper panel:* A selection of H₂ absorption lines from the $J = 0, 1, 2$ and 3 rotational levels from the $v = 0-1$ Lyman band. The model fit with parameters given in Table 2 is overplotted to the data as a dashed line. *Lower panel:* Detection of absorption lines from C⁰, C^{0*} and C^{0**} at $z_{\text{abs}} = 2.33771$ in the damped Lyman- α system. The model fit with parameters given in Table 1 is over-plotted to the data as a dashed line.







Hubble 1929

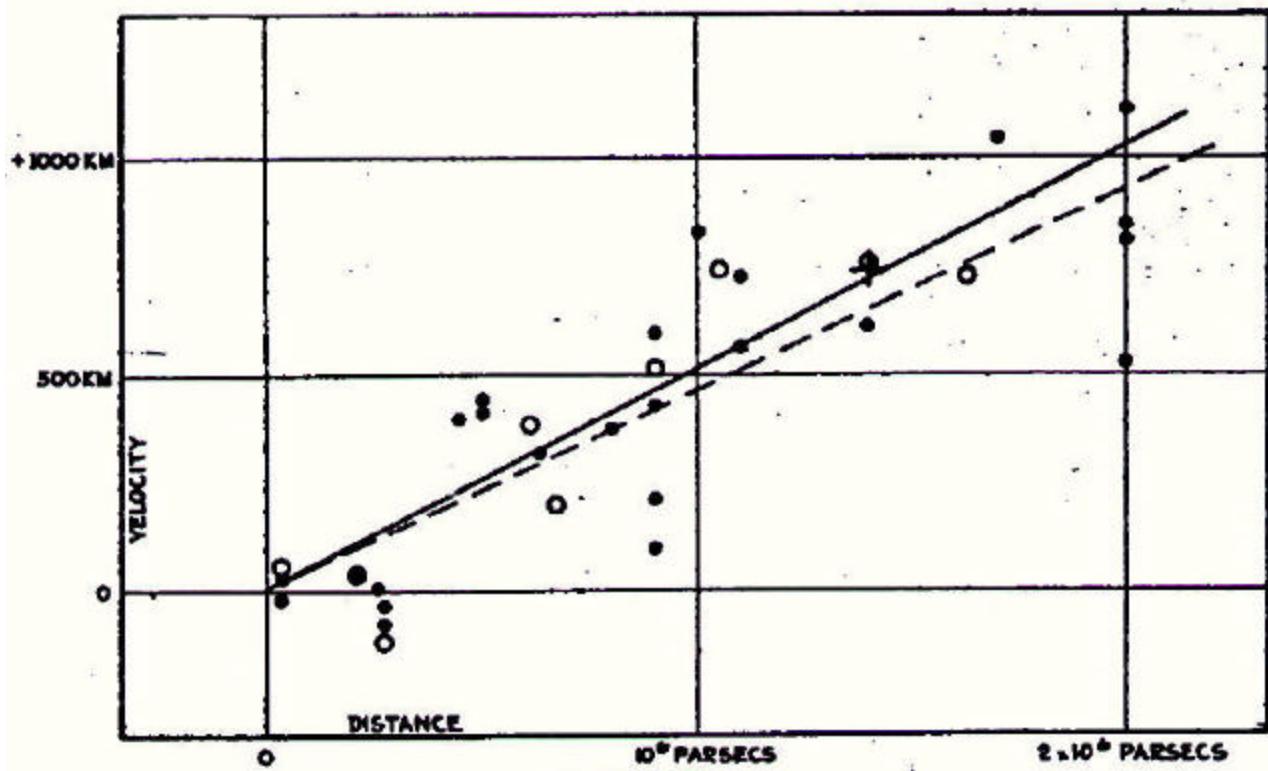


FIGURE 1